Proceedings of the 7th International Conference on Asian and Pacific Coasts (APAC 2013) Bali, Indonesia, September 24-26, 2013

SEDIMENT TRANSPORT CALCULATION CONSIDERING COHESIVE EFFECTS AND ITS APPLICATION TO WAVE-INDUCED TOPOGRAPHIC CHANGE

Y.H. Cho [1], T. Nakamura [2], N. Mizutani [3] and K.H. Lee [4]

ABSTRACT: A sediment transport calculation considering cohesive force is proposed to deal with the transport phenomena of cohesive sediment. In the proposed calculation, each sand particle is assumed to be surrounded by a thin layer of clay. The critical Shields parameter and bed-load sediment transport rate are modified to include the cohesive force acting on the sand particle. The proposed calculation is incorporated into a two-way coupled fluid-structure-sediment interaction model, and applied to wave-induced topographic change of an artificial shallow. Numerical results show that an increase in the content ratio of the clay, cohesive resistance force per unit surface area and water content cause increases in the critical Shields parameter and decreases in the bed-load sediment transport rate, reducing the topographic change of a shallow without changing its trend. This suggests that mixing clay in the pores of the sand particles can reduce the topographic change of shallows.

Keywords: Cohesive force, fine sediment, sediment transport, shallow, numerical analysis

INTRODUCTION

Dredging is a periodically required activity in coastal and fluvial regions with the purpose of maintaining sea routes, environment protection and reservoir capacity. River channel and harbor dredging produces millions of tons of soil annually. Managing these enormous amounts of dredged soil remains an unsolved problem. One of the proposed methods of handling dredged soil is to create an artificial shallow in a nearby bay. From an environment perspective, it was confirmed that there are beneficial effects such as increasing bottom life and enhancing water purification potential (Kazama et al. 2006). In contrast, the stability of an artificial shallow composed of dredged soil against incident waves is of concern because of the low weight of fine sediments in the dredged soil. Nakamura et al. (2012a, 2012b) conducted experimental and numerical research on the characteristics of the topographic change of a shallow comprised of fine sand. However, these studies had limitations because they only considered non-cohesive fine sand, whereas actual dredged soil contains fine sediments with cohesive forces. Thus, there is little understanding of the characteristic of cohesive fine sediment transport and the topographic change of an artificial shallow made up of dredged soil.

Most research on sediment transport phenomena has been based on non-cohesive sediments and there is little research that accounts for the effects of cohesive forces. Ashida et al. (1982) proposed a formula concerning the non-dimensional critical shear stress and the non-equilibrium sediment transport of the sand particles. This formula considered the effects of the fine sediments (hereinafter called clay) with cohesive force existing in the pore space of the sand particles and confirmed the validity of the formula through comparison with experimental tests. However, there was no attempt to apply the formula to wave fields, which is a more energetic environment, to analyze the characteristics of sediment transport covering the cohesive effects in mixed soil coexisting with sand and clay such as dredged soil or the real sea bottom. Consequently, the characteristics of sediment transport in mixed soil are not fully understood, particularly in a coastal field of study.

In this study, a sediment transport calculation considering the cohesive effects induced by clay in the pores of sand particles is proposed and the basic characteristics of the calculation are investigated taking into account the correlation between cohesive intensity and the bed-load sediment transport rate. In addition, the calculation is incorporated into a three-dimensional coupled fluid-structure-sediment interaction model (FSSM) developed by Nakamura et al (2011), which can analyze the interaction between waves and topographic change, and applied to the condition of hydraulic experiments on the topographic change of a shallow composed of fine sand (Nakamura et al. 2012a). Furthermore, the predictive capability of the modified model is verified with experimental results and a

[1] Department of Civil Engineering, Nagoya University, Furo-cho, Chikusa-ku, Nagoya 464-8603, JAPAN
[2] Institute for Advanced Research, Nagoya University, Furo-cho, Chikusa-ku, Nagoya 464-8601, JAPAN
[3] Department of Civil Engineering, Nagoya University, Furo-cho, Chikusa-ku, Nagoya 464-8603, JAPAN
[4] Maritime & Ocean Engineering Research Institute, KIOST, Yuseong-daero, Yuseong-gu, Daejeon 305-343, KOREA

sensitivity analysis is carried out in terms of the effects of cohesive force on the topographic change of the shallow, which comprises a soil mixture based on the assumption that clay exists in the pores of the sand particles.

SEDIMENT TRANSPORT CALCULATION CONSIDERING COHESIVE EFFECTS

Sediment transport calculation considering the effects induced by clay contained in the pores of the sand particle is proposed following Ashida et al. (1982). Specifically, the critical Shields parameter τ_{*c} and bed-load sediment transport rate q_i are modified to consider the cohesive effects of the clay.

Ashida et al. (1982) considered the soil mixture combined with spherical sand particles with uniform particle diameter d_{50} and clay filling in the pores of the sand particles as bottom sediment. It was assumed that the friction between the sand particles did not change even for the condition without clay. That is, even though the clay is eliminated, sand particles can maintain a static stable state. Thus, we now have the clay-induced cohesive force F_C expressed by:

$$F_C = k_1' d_{50}^2 f_c , \tag{1}$$

in which $k_1' d_{50}^2$ is the cohesive area of the clay contributing to the cohesive resistance and f_c is the cohesive resistance force of the clay per unit surface area. Here, assuming the cohesive area per contact point between sand particles is a, it can be obtained approximately from a simple geometric relationship as in Ashida et al. (1982). When one sand particle is supported by the number of contact points, n, this can be given by $k_1' d_{50}^2 = an$, and finally, Eq. (1) can be expressed as:

$$F_C = \frac{\pi d_{50}^2}{4}\left[\left\{1+\frac{1}{1-m}\frac{p_f(1+s\omega)}{p_f s\omega+1}\right\}^{2/3}-1\right] n f_c , \tag{2}$$

in which m is the porosity; p_f is the content ratio of the clay; ω is the water content; and s is the specific weight of the sand particle (= ρ_s/ρ_w, where ρ_s is the sand particle density and ρ_w is the water density). Additionally, there are the submerged weight of the particle, W, and the drag and lift forces, F_D and F_L, which are triggered by the bottom velocity. The forces acting on the sand particles, apart from the cohesive force F_C expressed in Eq. (2), are expressed by:

$$W = \frac{1}{6}\pi(\rho_s-\rho_w) g d_{50}^3 , \tag{3}$$

$$F_D = \frac{1}{8}\pi\varepsilon C_{D1}\rho_w d_{50}^2 v_r^2 = C_{FD} v_r^2 , \tag{4}$$

$$F_L = \frac{1}{8}\pi\varepsilon C_L\rho_w d_{50}^2 v_r^2 = k_L C_{FD} v_r^2 , \tag{5}$$

in which g is the gravitational acceleration; ε is the shading coefficient; C_{D1} and C_L are the turbulent drag and lift coefficients; k_L is the ratio between C_{D1} and C_L (= C_L/C_{D1}); v_r is the relative flow velocity acting on the particle for the mean transport velocity v_b of a sediment particle in bed-load motion; and $C_{FD} = \pi\varepsilon C_{D1}\rho_w d_{50}^2/8$. In the following, τ_{*c} and q_i are derived by incorporating the effects of F_C.

Critical Shields Parameter

In the critical state, the force acting on a sand particle exists as shown in Fig. 1. Here, v_f is the friction velocity; C_{vf} is the coefficient of the friction velocity; α is the angle between the flow velocity $C_{vf}v_f$ and the direction of the steepest bed slope; Ψ is the angle between the flow velocity $C_{vf}v_f$ and the sediment transport velocity v_b; and Ψ_1 is the angle between the relative flow velocity v_r and the sediment transport velocity v_b. The values F_{DC}, F_{LC}, v_{fc}, v_{bc}, v_{rc}, α_c, Ψ_c and Ψ_{1c} represent those of F_D, F_L, v_f, v_b, v_r, α, Ψ and Ψ_1 in the critical state. In addition, β is the angle of the steepest bed slope and μ_s is the static friction coefficient of the sand particle. In this case, $v_{bc} = 0$, which means that $v_{rc} = C_{vf}v_{fc}$ and $\Psi_c = \Psi_{1c}$, because it is under the critical state. The formulations of Ψ_c and v_{rc}^2 are given as follows from the force balance in the directions the same as and perpendicular to v_{bc}:

$$v_{rc}^2 = \frac{\{\mu_s\cos\beta-\sin\beta\cos(\alpha_c-\Psi_c)\}W+F_c}{(\cos\Psi_c+\mu_s k_L)C_{FD}} , \tag{6}$$

$$\Psi_c = \arctan\left\{\frac{W\sin\beta\sin\alpha_c}{C_{FD}v_{rc}^2+W\sin\beta\cos\alpha_c}\right\} . \tag{7}$$

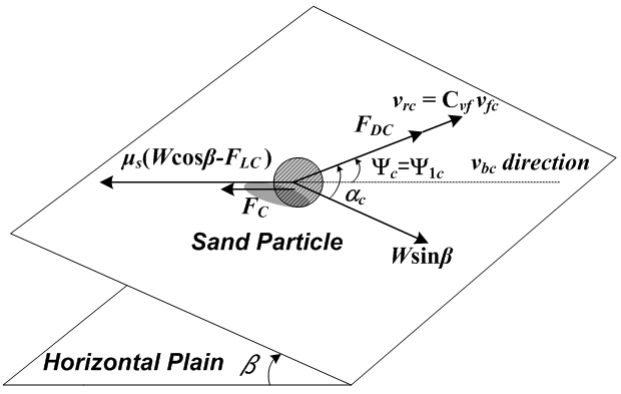

Fig. 1 Force balance on a sediment particle on a sloping bed in the critical state

In Eq. (7), Ψ_c and α_c have the same sign and $|\Psi_c| \le |\alpha_c|$. Here, the unknown parameters, v_{rc}^2 and Ψ_c, are determined by iterative calculations. Defining τ_{*c0} as a critical Shields parameter in the horizontal plane ($\beta = 0$) without considering the cohesive force ($F_C = 0$), τ_{*c} can be written by the following equation:

$$\frac{\tau_{*_c}}{\tau_{*c0}} = \frac{v_{fc}^2 / \{(s-1)gd_{50}\}}{v_{fc0}^2 / \{(s-1)gd_{50}\}} = \frac{v_{rc}^2 / \{C_{vf}^2 (s-1)gd_{50}\}}{v_{rc0}^2 / \{C_{vf}^2 (s-1)gd_{50}\}} = \frac{v_{rc}^2}{v_{rc0}^2}, \quad (8)$$

in which v^2_{rc0} and v^2_{fc0} are v^2_{rc} and v^2_{fc} in the horizontal plane ($\beta = 0$) without the cohesive force ($F_C = 0$), and v^2_{rc0} is obtained as follows from substituting $F_C = \beta = \Psi_c = \Psi_{1c} = 0$ into Eq. (6):

$$v_{rc0}^2 = \frac{\mu_s W}{(1+\mu_s k_L) C_{FD}}. \quad (9)$$

Furthermore, for the cross-sectional two-dimensional phenomenon, the following equation is obtained because of $\alpha_c = \Psi_c = \Psi_{1c} = 0$:

$$\frac{\tau_{*_c}}{\tau_{*c0}} = \frac{(\mu_s \cos\beta - \sin\beta) W + F_c}{\mu_s W}. \quad (10)$$

In addition, the influence of the cohesive force is considered to be a pickup function of suspended sediment through the value of the critical Shields parameter τ_{*c}.

Bed-Load Sediment Transport Rate

The bed-load sediment transport rate q_i per unit width and unit time is defined as follows (Engelund and Fredsøe 1976):

$$q_i = \frac{1}{6} \pi d_{50} p_{EF} v_{bi}, \quad (11)$$

where p_{EF} is the percentage of sediment particles in bed-load motion in the surface layer of the bed, which is expressed as:

$$p_{EF} = \begin{cases} 0 & \text{if} \quad \tau_* \le \tau_{*_c} \\ \dfrac{6}{\pi \mu_d} (\tau_* - \tau_{*_c}) & \text{if} \quad \tau_* > \tau_{*_c} \end{cases}, \quad (12)$$

in which μ_d is the dynamic friction coefficient ($\mu_d \le \mu_s$) and τ_* is the Shields parameter, which is defined as:

$$\tau_* = \frac{v_f^2}{(s-1)gd_{50}}. \quad (13)$$

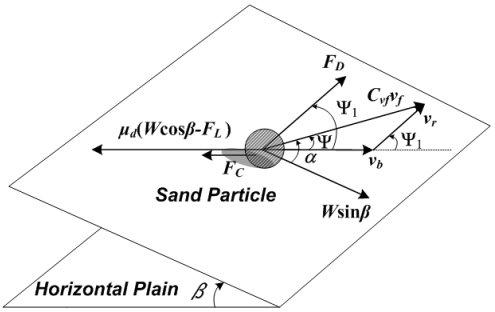

Fig. 2 Force balance on a moving sediment particle on a sloping bed

Figure 2 shows the agitating and stabilizing forces acting on a sand particle in the bed-load motion. The equation of motion in the same direction as the sand particle movement (i.e., the direction of v_b) is given as:

$$\begin{aligned} F_D \cos\Psi_1 + W \sin\beta \cos(\alpha - \Psi) \\ = \mu_d (W \cos\beta - F_L) + F_c \end{aligned}. \quad (14)$$

In the same way, the equation of motion in the direction perpendicular to the sand particle movement is:

$$F_D \sin\Psi_1 = W \sin\beta \sin(\alpha - \Psi). \quad (15)$$

In addition, the simple geometric relationship between v_b, $C_{vf}v_f$ and v_r gives:

$$v_r \sin\Psi_1 = C_{vf} v_f \sin\Psi, \quad (16)$$

$$v_r \cos\Psi_1 + v_b = C_{vf} v_f \cos\Psi. \quad (17)$$

Here, there are four unknown variables (i.e., v_b, v_r, Ψ and Ψ_1) and four equations, and v_{bi} is computed through iterative calculations. Thus, the bed-load sediment transport rate q_i is given by Eqs. (11) and (12) together with τ_{*c}, which is obtained in the previous section. Furthermore, for the cross-sectional two-dimensional phenomenon, the equation is summarized as follows from the relationship of $\alpha = \Psi = \Psi_1 = 0$:

$$v_b = C_{vf} v_f - v_r, \quad (18)$$

$$v_r = \left\{ \frac{(\mu_d \cos\beta - \sin\beta) W + F_c}{C_{FD}(1+\mu_d R_L)} \right\}^{1/2}. \quad (19)$$

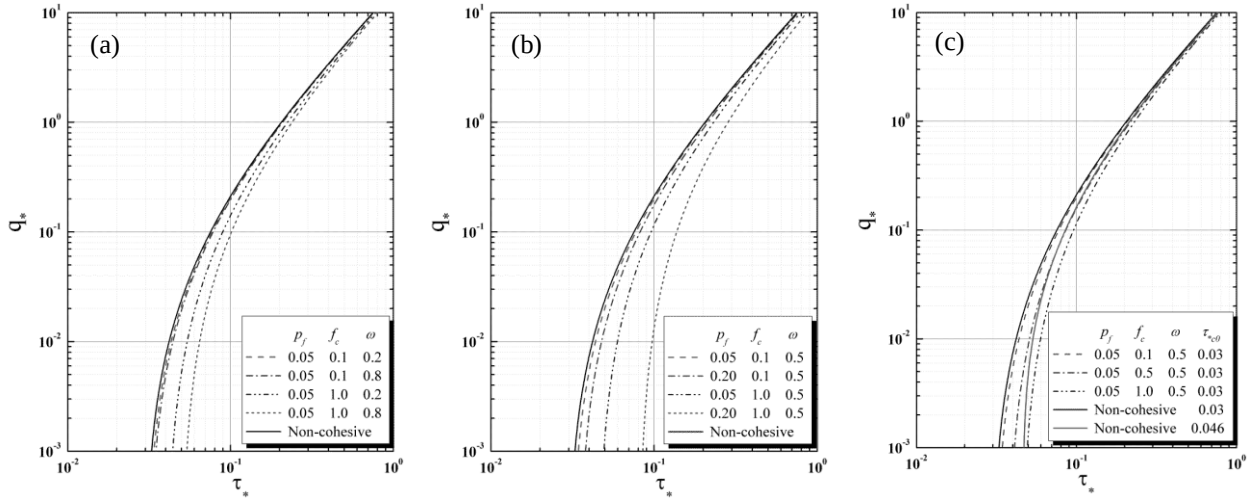

Fig. 3 Non-dimensional bed-load sediment transport rate q_* versus the Shields parameter τ_*: (a) the characteristic of q_* according to ω; (b) the characteristic of q_* according to p_f; and (c) the characteristic of q_* according to f_c

CHARACTERISTICS OF SEDIMENT TRANSPORT CALCULATION CONSIDERING COHESIVE EFFECTS

In this section, the fundamental characteristics of the proposed sediment transport calculation are investigated based on Eqs. (10), (18) and (19) for a cross-sectional two-dimensional condition, for which there is no need to perform any iterative calculation. Specifically, sand particles with d_{50} = 0.1 mm, $\rho_s = 2.65\times10^3$ kg/m^3 and τ_{*c0} = 0.03 were assumed to be on the horizontal plane ($\beta = 0°$). The three cases for the water content ω (0.2, 0.5 and 0.8), two cases for the content ratio of the clay p_f (0.05 and 0.20) and three cases for the cohesive force per unit surface area f_c (0.1, 0.5 and 1.0 N/m^2) were then used as the main variables. The calculation without the cohesive force effect (f_c = 0.0 N/m^2) was also carried out for comparative analysis. Other parameters were g = 9.80 m/s^2, $\rho_w = 9.97\times10^2$ kg/m^3, C_{D1} = 0.45, C_{vf} = 10.0, k_L = 0.85, ε = 0.4, μ_s = 0.63 and μ_d = 0.51, which are the same as used in Nakamura et al. (2011).

Figure 3 shows the relationship of the non-dimensional bed-load sediment transport rate q_* versus the Shields parameter τ_*. As shown in Fig. 3(a), an increase in ω causes an increase in the critical Shields parameter τ_{*c}. In addition, it is observed that q_* tends to decrease with an increase in ω when τ_* is the same. However, the effect of ω on q_* varies according to the value of f_c because the decline in q_* increases with an increase in f_c. A similar phenomenon is also observed in Fig. 3(b). Although a decrease in q_* according to an increase in p_f is small for f_c = 0.1 N/m^2, it is found that a decline in q_* for f_c = 1.0 N/m^2 is larger than that for f_c = 0.1 N/m^2 (see Fig. 3(b)). In Fig. 3(c), the value of τ_{*c} increases with an increase in f_c, and it is also found that q_* decreases with an increase in f_c for the same τ_*. Furthermore, the case of τ_{*c0} = 0.046, which is the solid green line without cohesive effects (f_c = 0.0 N/m^2), and the case of f_c = 1.0 N/m^2 and τ_{*c0} = 0.03, which is the blue two-dot chain line, are compared based on the same critical Shields number τ_{*c} because τ_{*c} is about 0.046 when f_c = 1.0 N/m^2 and τ_{*c0} = 0.03. A different trend in q_* is observed in spite of the same critical Shields parameter, that is, q_* for f_c = 1.0 N/m^2 is smaller than that for non-cohesive effect consideration. This result emphasizes the importance of appropriate modeling taking into account the cohesive effects caused by the clay in sediment transport calculation because considering only the increasing effects of τ_{*c0} caused by the cohesive force is insufficient.

THREE-DIMENSIONAL COUPLED FLUID-STRUCTURE-SEDIMENT INTERACTION MODEL

The three-dimensional coupled fluid-structure-sediment interaction model developed by Nakamura et al. (2011) is briefly described in this section. The model is composed of a main solver and three modules. The main solver is a large-eddy simulation (LES) based on a continuity equation and a Navier-Stokes equation for analyzing the motion of an incompressible viscous air-water two-phase fluid including the pore fluid inside the porous media taking into account the movement of the movable structure and topographic change. The three modules are a volume-of-fluid (VOF) module based on the multi-interface advection and reconstruction solver (MARS) to track the gas-liquid interface, an immersed-boundary (IB) module based on the body-force type of IB method dealing with the movable structure, and the sediment transport module to analyze the concentration of suspended sediment transport and the topographic change associated with bed-load and suspended sediment

transport. The three modules are incorporated into the main solver with a two-way coupling technique to take into account the fluid-structure-sediment interaction. Here, the proposed sediment transport calculation was applied into the sediment transport module to take into account the cohesive effects caused by clay filling in the pores of the sand particles. It should be noted that, in this study, the IB module was not included because motion of the structure was not dealt with.

APPLICATION OF THE MODIFIED MODEL CONSIDERING COHESIVE EFFECTS

The modified model was applied to hydraulic experiments on the topographic change of an artificial shallow consisting of fine sand (Nakamura et al. 2012a) and its predictive capability was verified by comparison with experimental results. Subsequently, a numerical simulation was carried out on the supposed condition that the pores of the sand particles contained the clay with the cohesive force, and the sensitivity analysis of the modified model was conducted focusing on the relationship between the variation of the parameters (f_c, p_f, ω) and topographic change of the shallow.

Verification of The Modified Model

Numerical condition

Figure 4 shows a schematic of a computational domain. As shown in Fig. 4, a shallow (height: 20.0 cm; crown width: 200.0 cm; slope gradient: 1/20) composed of fine sand with a median grain size, d_{50} = 0.1 mm, was installed based on the initial topography measured in the hydraulic experiments. In addition, a wave generating source/sink was placed 140.0 cm away from the beginning of the shallow, and damping zones were installed in the offshore side of the wave generating source and the onshore side of the vertical wall. Here, the length of the damping zones was about twice as long as the incident wavelength to reduce the wave reflection from the boundaries. Regular waves were generated with a wave height H_i = 6.5 cm, a wave period T = 1.0 s, and a still water depth h = 22.50 cm. The entire domain except for the damping zones was discretized using orthogonal staggered cells with a uniform size of Δx = 2.0 cm and Δz = 0.5 cm, whereas non-uniform cells widening gradually were used in the damping zones for efficient numerical simulation. The boundary conditions were the same as in Nakamura et al. (2012b). The parameters were the porosity of fine sand m = 0.4, the density $\rho_s = 2.65\times10^3$ kg/m^3, the critical Shields parameter on the horizontal plane τ_{*c0} = 0.03, the submerged angle of repose $\theta_r = 30.0^\circ$ and the content ratio of the clay p_f = 0.0 because the shallow was composed of only fine sand without clay. Other parameters were referred to in the previous section and Nakamura et al. (2011).

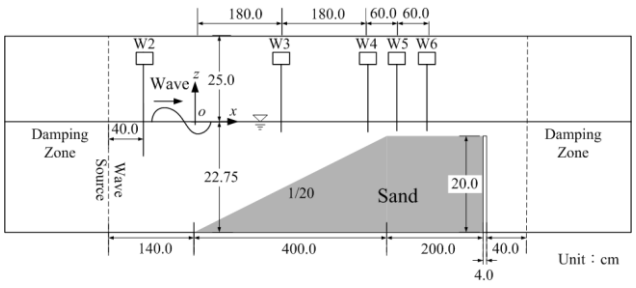

Fig. 4 Computational domain for the topographic change of the shallow

Predictive capability of the modified model

Although the topographic changes have been measured in the hydraulic experiments at 1, 10, 30, 60 and 300 min after the waves were generated, only the result of the topographic change with t = 1 min was adopted in this study to avoid the heavy computational load and impractical work from long simulation times of over 10 min.

The comparison between experimental and numerical results for free surface elevations η observed from W2 to W6 (see Fig. 4) is presented in Fig. 5, in which t denotes time. As shown in Fig. 5, although a slight phase shift was observed for W2 located at the offshore side of the shallow and W3 at the middle of the seaward slope of the shallow, reasonable results were obtained. A decrease in the wave height, which occurred subsequent to wave breaking, is shown from the upper slope (W4) to the crown of a shallow (W6), and the amplitude η has

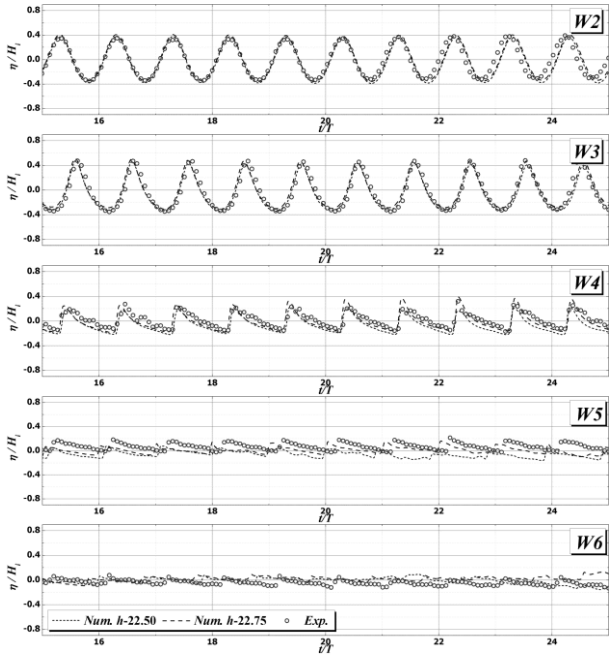

Fig. 5 Comparison between experimental (circle) and numerical (dotted line) results for free surface elevation η

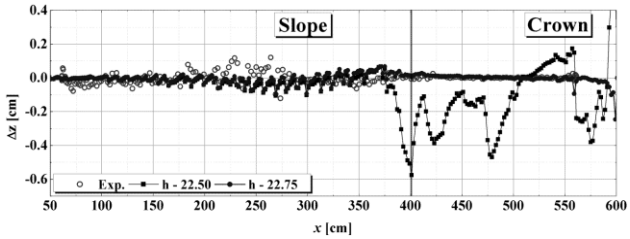

Fig. 6 Comparison of the amount of topographic change Δz between experimental (circle) and numerical results (solid line) at t = 60 s

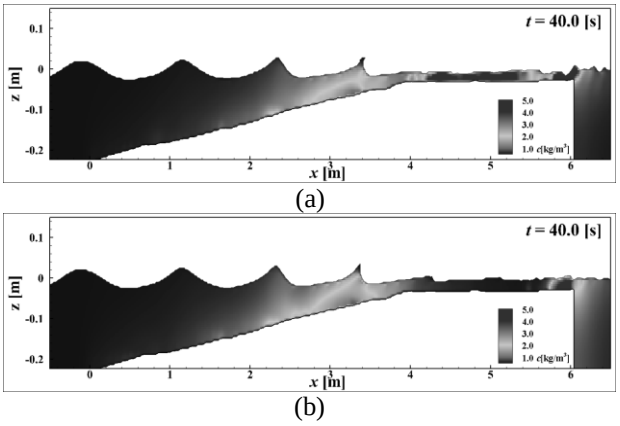

Fig. 7 Topographic change and the suspended sediment concentration at t = 40 s for the different still water depths: (a) h = 22.50 cm; (b) h = 22.75 cm

reasonably good agreement. However, especially at W5, there is the tendency for the mean water depth to vary as time passes. This is because, in the hydraulic experiments, the 0.40 m wide wave flume was designed by dividing the 2.22 m wide wave tank with a partition board, and the shallow mentioned above was installed on the 0.40 m wide wave flume. In this case, circulation flow can be generated by the mean water depth variation in the wave tank, which affected the experimental results because the partition board did not extend adequately to the wave absorbing beach at the end of the wave tank. Thus, it seemed that a discrepancy between the numerical and experimental results for W4 to W6, particularly in a low water depth area, was evident because a cross-sectional two-dimensional simulation used in this study has the restriction of reproducing completely the phenomena that emerged in the three dimensional experiments. This dimensional limitation is also reflected in the numerical results for the topographic change. Figure 6 shows the experimental and numerical results of the topographic change Δz of the shallow at t = 60 s, where a positive value of Δz indicated deposition. It shows that when the water depth of 22.50 cm, the same as the experimental condition, was adopted for the numerical simulation (black solid line), substantial erosion took place on the upper slope to the middle of the crown, which was different from the experimental results. Note that similar results were also obtained in a previous study (Nakamura et al. 2012b). From this result, it can be considered that the trend for the topographic change altered because of the mean water variation, especially the phenomenon of an increase in mean water depth in the experiment at W5.

Consequently, the numerical simulation was conducted by raising the water depth slightly to enhance the predictive capability of the model in the hydraulic experiments for the cross-sectional two-dimensional calculation. As a result, when the water depth was raised to 22.75 cm, 0.25 cm deeper than the experiments, the predictive accuracy of η at W4 and W5 was improved as shown in Fig. 5 and overall the trend for the free surface elevations corresponded to that for the experimental results. Moreover, the correlation with the experimental results was improved in terms of the topographic changes because there was no significant topographic change, especially for the erosion that occurred in the slope to the crown (see Fig. 6) unlike the case for h = 22.50 cm. These results for the different topographic change patterns were also obvious in the suspended sediment concentration results (see Fig. 7). The red contour indicates a high concentration of suspended sediment and the blue contour means the reverse. From Fig. 7(b), some suspended sediment was observed in the upper slope and at the end of the crown, the same as shown in Fig. 7(a). However, when h = 22.50 cm (Fig. 7(a)), high suspended sediment concentration was observed on the crown of the shallow as shown in Fig. 6, whereas there was little suspended sediment on the crown with h = 22.75 cm (Fig. 7(b)).

Consequently, it was established that this model was applicable to the topographic change phenomena of a shallow, since the predictive capability of the model was verified by raising the water depth to 22.75 m. Therefore, in the following, the sensitivity analysis for the main parameters (f_c, ω and p_f) contributing to cohesive force was carried out with h = 22.75 cm to investigate the effects of the cohesive force on the topographic changes of the shallow.

Effects of The Cohesive Force on The Topographic Changes of a Shallow

It is assumed that clay filled the pores of the sand particles forming the shallow. The cohesive resistance force per unit surface area f_c, the water content ω and the content ratio of the clay p_f are noted as the main parameters which lead to cohesive force, and the effects of these parameters on the topographic change of the shallow were investigated.

The effects of f_c, ω and p_f on the topographic change Δz at t = 60 s are shown in Fig. 8. In the figure, only Δz

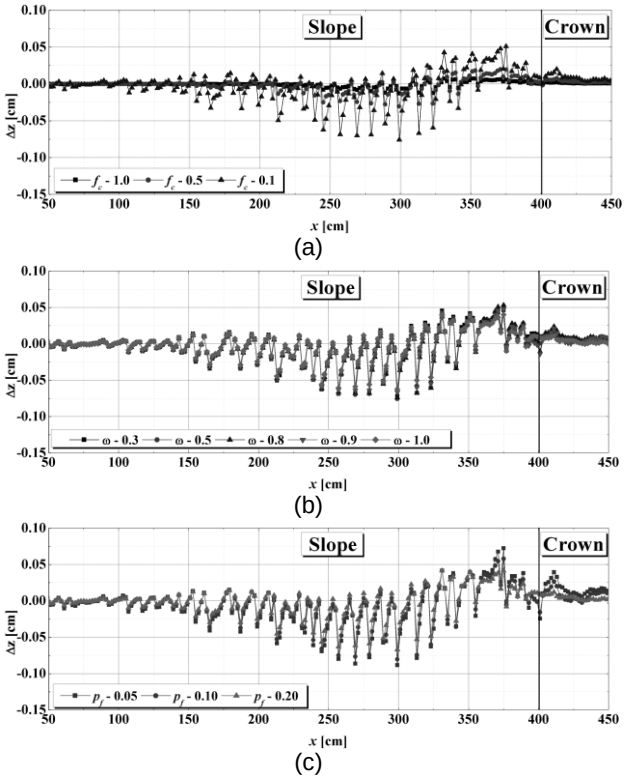

Fig. 8 Difference in the amount of topographic change Δz caused by the cohesive force at t = 60 s: (a) the effects of the cohesive force per unit surface area (ω = 0.5, p_f = 0.15); (b) the effects of the water content (p_f = 0.15, f_c = 0.1 N/m^2); (c) the effects of the content ratio of the clay (ω = 0.5, f_c = 0.1 N/m^2)

in the range of x = 50–450 cm of the whole domain was expressed because the topographic change mainly occurred on the slope of the shallow as shown in Fig. 6. It was confirmed from Fig. 8(a) that the amount of Δz tends to decrease with an increase in f_c. Specifically, when f_c was increased from 0.1 N/m^2 to 1.0 N/m^2, it was observed that little deposition emerged on the location from the upper slope to the crown and little erosion appeared on the middle of the slope. This was because, as shown in Fig. 3(c), the critical Shields parameter increased and the bed-load sediment transport rate decreased with an increase in f_c, and finally this sequence had the effect of decreasing Δz. In addition, although Δz decreased with an increase in ω, the distinction was very small as shown in Fig. 8(b). This was because the small value of f_c, 0.1 N/m^2, was adopted on account of the little topographic change that occurred for f_c = 1.0 N/m^2, and the effects of ω on the critical Shields parameter and the bed-load sediment transport rate were very small when f_c = 0.1 N/m^2 as shown in Fig. 3(a). A similar trend to that shown in Fig. 8(b) is also observed in Fig. 8(c). Furthermore, the variation of the parameters f_c, ω and p_f seems to have little effect on the trend for the topographic change of the shallow. Therefore, by filling the pores of the sand particles with clay, the wave-induced topographic change of the shallow can be reduced without changing the topographic change pattern.

CONCLUSIONS

In this study, the sediment transport calculation considering the cohesive force generated by clay filled sand particles was proposed. The numerical simulation model incorporating the proposed calculation was verified by applying it to the hydraulic experiments on the topographic change of a shallow composed of fine sand, and the basic characteristics of the model were examined. In addition, the validation of the model and the sensitivity analysis of the cohesive effects on the topographic change of the shallow were conducted. As a result, the conclusion can be summarized as follows:

1. Through the relationship between the non-dimensional bed-load sediment transport rate and Shields parameter, an increase in the cohesive resistance force per unit surface area f_c, the water content ω and the content ratio of the clay p_f result in an increase in the critical Shields parameter and a decrease in the bed-load sediment transport rate. Furthermore, the existence of clay in the pores of the sand particles indicates the importance of proper modeling taking into account the cohesive effects. This is because the results presented different patterns for the bed-load sediment transport rate for cases considering cohesive and non-cohesive effects, in spite of having the same critical Shields number.
2. By carrying out a sensitivity analysis on the effects of the three parameters, f_c, ω and p_f, on the topographic change of the shallow, it was confirmed that the topographic change was decreased with an increase in f_c ω and p_f. In addition, the results show that taking into account the cohesive effects had little influence on the topographic change pattern. Consequently, the possibility of reducing topographic change by containing the clay in the sand particles without any change in its trend is suggested.

From these results, the computational capability of this proposed model for analyzing sediment transport problems involving various conditions of mixed sediments coexisting with sand and clay was confirmed. However, it is desirable to validate the proposed calculations with hydraulic experiments.

ACKNOWLEDGEMENT

The authors are grateful for the financial support of the Steel Foundation for Environmental Protection Technology, Japan (SEPT).

REFERENCES

Ashida K., Egashira, S. and Kamoto, M. (1982). Study on the erosion and variation of mountain streams - on the erosion and transportation of sand-clay mixtures. Disaster Prevention Research Institute Annuals B, 25(B-2): 349-360 (in Japanese).

Engelund, G. and Fredsøe, J. (1976). A sediment transport model for straight alluvial channels. Nordic Hydrology, 7: 293-306.

Kazama, T., Nakata, K., Tanabe, Y., Hasegawa, M., Oshima, I. and Nagakura, T. (2006). Tidal flats and shallows created through the utilization of dredged sand and its effectiveness on coastal sea environment and its problem. Proc., JSCE in the Ocean, 22: 607-612 (in Japanese).

Nakamura T., Yim, S.C. and Mizutani, N. (2011). Numerical simulation on local scouring around bottom-mounted movable short cylinder. Proc., Coastal Structures 2011, ASCE, C4-087, 12p.

Nakamura, T., Nezasa, Y. and Mizutani, N. (2012a). Experimental study on evolution of surface profile of artificial shallow and temporal change in pore-water pressure inside surface layer of shallow. J. JSCE Series B2 (Coastal Eng.), 68: I_541-I_545 (in Japanese).

Nakamura, T., Ishihara, R. and Mizutani, N. (2012b). Numerical analysis of topographic change of artificial shallow considering pore-water pressure in surface layer of shallow. J. JSCE Series B2 (Coastal Eng.), 68: I_1161-I_1165 (in Japanese).